Eur. Phys. J. C 40, 435–445 (2005)
Digital Object Identifier (DOI) 10.1140/epjc/s2005-02148-6

THE EUROPEAN PHYSICAL JOURNAL C

Sneutrino production at e^+e^- linear colliders: addendum to slepton production

A. Freitas[1,a], A. von Manteuffel[2], P.M. Zerwas[2]

[1] Fermi National Accelerator Laboratory, Batavia, IL 60510-500, USA
[2] Deutsches Elektronen-Synchrotron DESY, 22603 Hamburg, Germany

Received: 10 September 2004 / Revised version: 11 October 2004 /
Published online: 3 March 2005 –

Abstract. Complementing the preceding study of charged scalar leptons, the sector of the neutral scalar leptons, sneutrinos, is investigated in a high-precision analysis for future e^+e^- linear colliders. The theoretical predictions for the cross-sections are calculated at the thresholds for non-zero widths and in the continuum including higher-order corrections at the one-loop level. Methods for measuring the sneutrino masses and the electron-sneutrino–gaugino Yukawa couplings are presented, addressing theoretical problems specific for the sneutrino channels.

1 Introduction

The precision analysis of charged scalar leptons (sleptons) at future high-energy e^+e^- and e^-e^- colliders has been studied for the first two generations in a preceding report [1], establishing precise theoretical calculations which include non-zero width and rescattering effects at the thresholds and the complete set of one-loop corrections in the continuum. The corresponding process of stau production, including mixing effects, has been discussed in [2].

In this addendum the work will be extended to the neutral slepton sector, i.e. the production of sneutrinos in e^+e^- annihilation,

$$e^+e^- \to \tilde{\nu}_l\tilde{\nu}_l^* \quad \text{for} \quad l = e, \mu, \tau. \tag{1}$$

Note that the $\tilde{\nu}_l$ are assumed to be the partners of the left-handed sneutrinos, since if the right-handed neutrino masses are close to the GUT scale, the R-sneutrino masses are expected to be so heavy [3] that mixing with the L-sneutrinos is irrelevant.

We will elaborate in particular the onset of the electron-sneutrino ($\tilde{\nu}_e$) cross-section near threshold, which allows for a determination of the $\tilde{\nu}_e$ mass. The accuracy of the mass measurement through threshold scans is superior to other methods using decay spectra of the sneutrinos produced in the continuum [4]. Belonging to the same iso-doublet, the masses of the sneutrinos and the L-sleptons are related by a sum rule involving the D-term of the supersymmetry (SUSY) Lagrangian. This symmetry relation can be tested stringently.

While sneutrino production of the second and third generation in e^+e^- collisions is mediated by s-channel Z-boson exchange, $\tilde{\nu}_e$ pair production in addition involves t-channel chargino exchange, thereby being sensitive to the electron-sneutrino-chargino $e^\mp\tilde{\nu}_e\tilde{\chi}^\pm$ Yukawa couplings. From the measurement of $\tilde{\nu}_e$ production one can therefore scrutinize the identity of the gauge and Yukawa couplings of the electroweak SU(2) sector.

To provide precise theoretical descriptions for sneutrino production, we have calculated the production cross-sections near threshold including non-zero width and off-shell effects, while in the continuum the complete one-loop corrections for on-shell sneutrino production are presented. The phenomenological analyses are based on the minimal supersymmetric standard model (MSSM), adopting as an example the Snowmass Point SPS1a [5]. Effects of initial-state beamstrahlung as well as decays of the sneutrinos are taken into account. The final results demonstrate that measurements of the $\tilde{\nu}_e$ sneutrino masses and of the $e\tilde{\nu}_e\tilde{W}$ couplings are possible at the per-cent level, supplementing the similarly precise picture of the charged slepton sector [1].

In Sect. 2 the general features of sneutrino production are summarized at leading order. Section 3 presents sneutrino-pair production at threshold and analyses the expected accuracies in threshold scans. In Sect. 4 the pair production of sneutrinos in the continuum is analyzed at the one-loop level, and applied for the determination of SUSY Yukawa couplings. Conclusions are summarized in Sect. 5.

2 Basics of smuon and selectron production and decay

For definiteness, the analysis is restricted to the minimal supersymmetric standard model (MSSM), including sneutrinos with chiral quantum number L, while R-sneutrinos

[a] e-mail: afreitas@fnal.gov

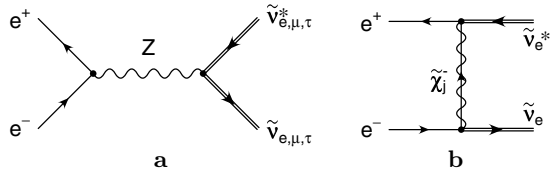

Fig. 1. Generic leading-order diagrams for the pair production of sneutrinos in e^+e^- annihilation

are assumed absent as argued before. We adopt the conventions and notation introduced in [1].

2.1 Production mechanisms

Muon- and tau-sneutrinos $\tilde{\nu}_{\mu,\tau}$ are generated in diagonal pairs via s-channel Z-boson exchange in e^+e^- collisions; see Fig. 1a. Electron-sneutrino $\tilde{\nu}_e$ pair production proceeds in addition through chargino $\tilde{\chi}_j^\pm$ $[j = 1 \ldots 2]$ exchanges in the t-channel, cf. Fig. 1a,b. Since only sneutrinos in with chiral index L are produced, the conservation of chiral quantum number in the interactions demands sneutrinos to be produced in P-wave states, for both s- and t-channel mechanisms near threshold. This leads to the characteristic β^3 onset of the excitation curves near threshold, with β denoting the velocity of the final-state sneutrinos.

The Born cross-sections for sneutrino production by polarized beams read

$$\sigma[e^+_{\rm R}e^-_{\rm L} \to \tilde{\nu}_l\,\tilde{\nu}_l^*] \qquad (2)$$
$$= \frac{2\pi\alpha^2}{3s}\beta^3\,\frac{(1-2{s_{\rm W}}^2)^2}{16{s_{\rm W}}^4{c_{\rm W}}^4}\left(\frac{s}{s-M_{\rm Z}^2}\right)^2 \quad [l=\mu,\tau],$$
$$\sigma[e^+_{\rm R}e^-_{\rm L} \to \tilde{\nu}_e\,\tilde{\nu}_e^*]$$
$$= \frac{2\pi\alpha^2}{3s}\beta^3\,\frac{(1-2{s_{\rm W}}^2)^2}{16{s_{\rm W}}^4{c_{\rm W}}^4}\left(\frac{s}{s-M_{\rm Z}^2}\right)^2$$
$$+\frac{\pi\alpha^2}{{s_{\rm W}}^4 s}\sum_{j=1}^{2}\sum_{k=1}^{2}|V_{j1}|^2\,|V_{k1}|^2\,h^{jk} \qquad (3)$$
$$+\frac{2\pi\alpha^2}{{s_{\rm W}}^2 s}\sum_{j=1}^{2}|V_{j1}|^2\,\frac{1-2{s_{\rm W}}^2}{4{s_{\rm W}}^2{c_{\rm W}}^2}\,\frac{s}{s-M_{\rm Z}^2}\,f^j,$$
$$\sigma[e^+_{\rm L}e^-_{\rm R} \to \tilde{\nu}_l\,\tilde{\nu}_l^*] = \frac{2\pi\alpha^2}{3s}\beta^3\,\frac{1}{4{c_{\rm W}}^4}\left(\frac{s}{s-M_{\rm Z}^2}\right)^2$$
$$[l=e,\mu,\tau], \qquad (4)$$
$$\sigma[e^+_{\rm R}e^-_{\rm R} \to \tilde{\nu}_l\,\tilde{\nu}_l^*] = \sigma[e^+_{\rm L}e^-_{\rm L} \to \tilde{\nu}_l\,\tilde{\nu}_l^*] = 0$$
$$[l=e,\mu,\tau], \qquad (5)$$

with

$$f^j = \Delta_j\beta - \frac{\Delta_j^2-\beta^2}{2}\,\ln\frac{\Delta_j+\beta}{\Delta_j-\beta}, \qquad (6)$$

$$h^{jk} = \begin{cases} -2\beta + \Delta_j \ln\dfrac{\Delta_j+\beta}{\Delta_j-\beta} & j=k, \\ \dfrac{f^k-f^j}{\Delta_j-\Delta_k} & j\neq k, \end{cases} \qquad (7)$$

where

$$\Delta_j = 2(m^2_{\tilde{\nu}_l} - m^2_{\tilde{\chi}_j^\pm})/s - 1 \quad \text{and} \quad \beta = \sqrt{1-4m^2_{\tilde{\nu}_l}/s}, \qquad (8)$$

and V_{ij} is the mixing matrix for positively charged charginos [1]. The electromagnetic coupling α should be taken at the scale $Q^2 = s$.

In the t-channel chargino exchange amplitudes, the contribution of the higgsino component of the chargino states can be neglected owing to the small electron-sneutrino–higgsino coupling proportional to the electron mass. The exchange of relatively light charginos with dominant gaugino component leads in general to electron-sneutrino production cross-sections that are more than an order of magnitude larger than for the other two flavors. Such a scenario is realized in the reference point SPS1a [5], as shown in Fig. 2.

The angular distributions for the sneutrino production processes with polarized beams read

$$\frac{{\rm d}\sigma}{{\rm d}\Omega}[e^+_{\rm R}e^-_{\rm L} \to \tilde{\nu}_l\,\tilde{\nu}_l^*] \qquad (9)$$

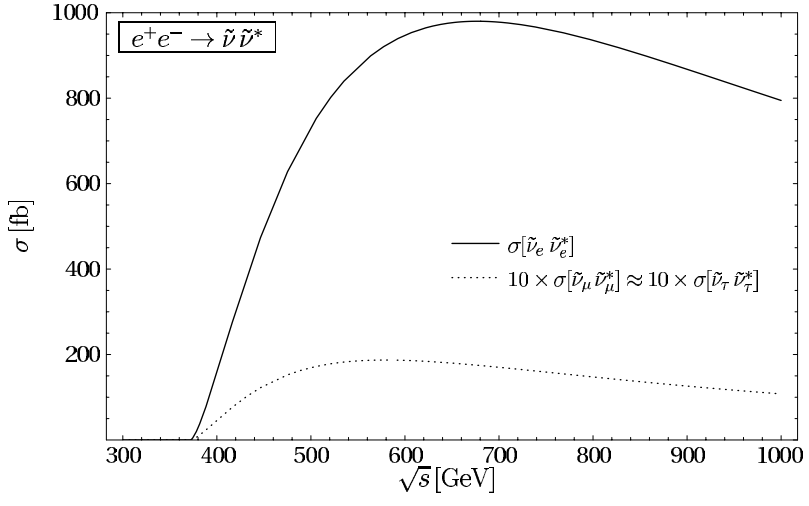

Fig. 2. Born cross-sections for sneutrino-pair production in unpolarized e^+e^- annihilation. The cross-section for $\tilde{\nu}_\tau$ production is very similar to the $\tilde{\nu}_\mu$ production cross-section. The mass values in the SPS1a scenario are collected in Table 1

$$= \frac{\alpha^2}{4s}\beta^3 \sin^2\theta \, \frac{(1-2{s_\mathrm{W}}^2)^2}{16{s_\mathrm{W}}^4{c_\mathrm{W}}^4} \left(\frac{s}{s-M_\mathrm{Z}^2}\right)^2 \quad [l=\mu,\tau],$$

$$\frac{\mathrm{d}\sigma}{\mathrm{d}\Omega}[e^+_\mathrm{R}e^-_\mathrm{L} \to \tilde{\nu}_e\,\tilde{\nu}_e^*]$$

$$= \frac{\alpha^2}{4s}\beta^3 \sin^2\theta \, \frac{(1-2{s_\mathrm{W}}^2)^2}{16{s_\mathrm{W}}^4{c_\mathrm{W}}^4} \left(\frac{s}{s-M_\mathrm{Z}^2}\right)^2$$
$$+ \frac{\alpha^2}{4{s_\mathrm{W}}^4 s}\beta^3 \sum_{j=1}^{2}\sum_{k=1}^{2} |V_{j1}|^2\,|V_{k1}|^2$$
$$\times \frac{\sin^2\theta}{\left[\Delta_j - \beta\cos\theta\right]\left[\Delta_k - \beta\cos\theta\right]} \qquad (10)$$
$$+ \frac{\alpha^2}{2{s_\mathrm{W}}^2 s}\beta^3 \sum_{j=1}^{2} |V_{j1}|^2 \frac{1-2{s_\mathrm{W}}^2}{4{s_\mathrm{W}}^2{c_\mathrm{W}}^2} \, \frac{s}{s-M_\mathrm{Z}^2} \, \frac{\sin^2\theta}{\Delta_j - \beta\cos\theta},$$

$$\frac{\mathrm{d}\sigma}{\mathrm{d}\Omega}[e^+_\mathrm{L}e^-_\mathrm{R} \to \tilde{\nu}_l\,\tilde{\nu}_l^*]$$

$$= \frac{\alpha^2}{4s}\beta^3 \sin^2\theta \frac{1}{4{c_\mathrm{W}}^4} \left(\frac{s}{s-M_\mathrm{Z}^2}\right)^2 \quad [l=e,\mu,\tau], \qquad (11)$$

with θ being the angle between the incoming e^- and the outgoing $\tilde{\nu}$ particles.

For muon- and tau-sneutrino production, the angular sparticle distributions follow the $\sin^2\theta$ rule typical for P-wave production. While near the threshold the angular distribution of electron-sneutrino production is also $\propto \sin^2\theta$, the t-channel chargino exchange amplitude peaks in the forward region near $\cos\theta \approx 1$ for high center-of-mass energies:

$$\frac{\mathrm{d}\sigma}{\mathrm{d}\cos\theta}[e^+\,e^- \to \tilde{\nu}_e\,\tilde{\nu}_e^*] \propto \sum_{j,k} \frac{1-\cos^2\theta}{\left[\Delta_j - \beta\cos\theta\right]\left[\Delta_k - \beta\cos\theta\right]}$$
$$\stackrel{s\gg m_{\tilde{\nu}}^2}{\longrightarrow} \frac{1+\cos\theta}{1-\cos\theta}, \qquad (12)$$

as expected from helicity analysis and t-channel exchange.

2.2 Decay mechanisms

The sneutrinos are typically expected to decay into light neutralino or chargino states with large gaugino components. The leading-order decay widths for these two-particle decays are given by

$$\Gamma[\tilde{\nu}_l \to \nu_l\,\tilde{\chi}_j^0] \qquad (13)$$
$$= \alpha\,|X_j|^2\,m_{\tilde{\nu}_l}\left(1 - \frac{m^2_{\tilde{\chi}_j^0}}{m^2_{\tilde{\nu}_l}}\right)^2 \qquad [i=\mathrm{L/R},\ j=1\ldots4],$$

$$\Gamma[\tilde{\nu}_l \to l^-\,\tilde{\chi}_k^+]$$
$$= \frac{\alpha}{4}|V_{k1}|^2\,m_{\tilde{\nu}_l}\left(1 - \frac{m^2_{\tilde{\chi}_k^\pm}}{m^2_{\tilde{\nu}_l}}\right)^2 \qquad [k=1,2], \qquad (14)$$

Table 1. Masses, widths and main branching ratios of sleptons and of the light neutralino and chargino states at Born level for the reference point SPS1a [5,6]

Sparticle	Mass m [GeV] Width Γ [GeV]	Decay modes	
$\tilde{l}_\mathrm{R} = \tilde{e}_\mathrm{R}/\tilde{\mu}_\mathrm{R}$	$m = 142.72$	$\tilde{l}_\mathrm{R}^- \to l^-\,\tilde{\chi}_1^0$	100%
	$\Gamma = 0.21$		
$\tilde{l}_\mathrm{L} = \tilde{e}_\mathrm{L}/\tilde{\mu}_\mathrm{L}$	$m = 202.32$	$\tilde{l}_\mathrm{L}^- \to l^-\,\tilde{\chi}_1^0$	48%
	$\Gamma = 0.25$	$\to l^-\,\tilde{\chi}_2^0$	19%
		$\to \nu_l\,\tilde{\chi}_1^-$	33%
$\tilde{\nu}_l = \tilde{\nu}_e/\tilde{\nu}_\mu$	$m = 185.99$	$\tilde{\nu}_l \to \nu_l\,\tilde{\chi}_1^0$	87%
	$\Gamma = 0.16$	$\to \nu_l\,\tilde{\chi}_2^0$	4%
		$\to l^-\,\tilde{\chi}_1^+$	10%
$\tilde{\nu}_\tau$	$m = 185.05$	$\tilde{\nu}_\tau \to \nu_\tau\,\tilde{\chi}_1^0$	89%
	$\Gamma = 0.15$	$\to \nu_\tau\,\tilde{\chi}_2^0$	3%
		$\to \tau^-\,\tilde{\chi}_1^+$	8%
$\tilde{\chi}_1^0$	$m = 96.18$	–	
$\tilde{\chi}_2^0$	$m = 176.62$	$\tilde{\chi}_2^0 \to \tilde{e}_\mathrm{R}^\pm\,e^\mp$	6%
	$\Gamma = 0.020$	$\to \tilde{\mu}_\mathrm{R}^\pm\,\mu^\mp$	6%
		$\to \tilde{\tau}_1^\pm\,\tau^\mp$	88%
$\tilde{\chi}_1^\pm$	$m = 176.06$	$\tilde{\chi}_1^+ \to \tilde{\tau}_1^+\,\nu_\tau$	100%
	$\Gamma = 0.014$		

where X_j and V_{kl} account for the neutralino and chargino mixings [1].

Masses, widths and branching ratios for the reference point SPS1a [5] are collected in Table 1. In the SPS1a scenario the decays into the lightest chargino and the second lightest neutralino, both of which are predominantly wino, are suppressed due to the small mass differences. As a consequence, the dominant channel is the decay into the bino-like lightest neutralino, leading to a completely invisible final state.

To obtain visible sneutrino-pair signals, we will therefore focus on the channel with one sneutrino decaying invisibly directly to the lightest neutralino, while the other sneutrino decays into a chargino and a charged lepton. Due to the relatively large value of $\tan\beta = 10$ in SPS1a and the large stau mixing, charginos decay almost completely into a τ final state. As a result, the physical signal for sneutrino production in this channel consists of a charged lepton with the sneutrino flavor $l = e,\mu,\tau$, one (additional) τ with opposite charge, and missing energy, $e^+e^- \to l^\pm\tau^\mp + \not{E}$. For $\tilde{\nu}_e$ and $\tilde{\nu}_\mu$ production this leads to a clear detector signature with an overall branching ratio of 17%. However, the analysis for $\tilde{\nu}_\tau$ production is experimentally very demanding, since only a pair of tau leptons is generated in the final state, with large backgrounds from two-photon interactions and other supersymmetric processes such as direct stau pair production.

3 Threshold production and mass measurements

As a consequence of chiral quantum number and angular momentum conservation, all sneutrino pairs are produced in e^+e^- annihilation near threshold in P-waves for both the s-channel and t-channel exchange mechanisms. This leads to the characteristic β^3 behavior of the excitation curve as a function of the velocity β of the produced particles. Since the produced sparticles are neutral, no Coulomb rescattering effects enhance the cross-sections at the thresholds.

When studying non-zero width effects, the off-shell production of the sneutrinos requires the analysis of the complete resonance decays and the corresponding continuum backgrounds with the same final states, i.e. the process

$$e^+e^- \to l^{\pm\,(-)}\!\!\nu_l\ \tilde{\chi}_1^0\,\tilde{\chi}_1^{\mp}, \tag{15}$$

including all Feynman diagrams leading to this final state.

The theoretical and phenomenological analysis of the threshold cross-sections for sneutrino production makes use of the methods set up in [1,7,8] for charged sleptons. As pointed out already in [9], due to the small production cross-section for muon- and tau-sneutrino production together with the possibly suppressed branching ratio into the final state $l^{\pm\,(-)}\!\!\nu_l\,\tilde{\chi}_1^0\,\tilde{\chi}_1^{\mp}$, the expected event rates near threshold are too low to perform a mass measurement from a threshold scan. For electron-sneutrino production, on the other hand, the signal rates are sufficiently high to allow a statistically significant threshold mass measurement. Subtracting the background cross-section by extrapolation from energies below threshold, the onset of the sneutrino excitation curve is in general sharp enough to determine precisely the sneutrino mass independent of the absolute normalization of the signal cross-section. This can be realized operationally by performing a multi-parameter fit including the overall normalization as a free variable. Within this frame the threshold production will be analyzed in the following for electron-sneutrinos.

The leading contribution to the $e^{\pm\,(-)}\!\!\nu_e\tilde{\chi}_1^0\,\tilde{\chi}_1^{\mp}$ final states is given by the double-resonance diagram shown in Fig. 3a. The non-zero sneutrino width $\Gamma_{\tilde{\nu}}$ is incorporated by shifting the mass in the sneutrino propagators into the complex plane, $m_{\tilde{\nu}}^2 \to M_{\tilde{\nu}}^2 = m_{\tilde{\nu}}^2 - \mathrm{i}m_{\tilde{\mu}}\Gamma_{\tilde{\nu}}$. To keep the amplitude gauge invariant, the double-resonance diagram of Fig. 3a must be supplemented by the single-resonance diagrams of Fig. 3b. In addition to the s-channel Z-exchange diagrams shown in the figure, there exist corresponding diagrams with t-channel chargino exchange.

Besides the signal sneutrino channels, the final state in the general process $e^+e^- \to e^{\pm}\tau^{\mp} + \not{E}$ receives backgrounds from a large variety of other processes. Within the SUSY sector itself, the main background arises from selectron pair production $\tilde{e}_{\mathrm{R}}^{\pm}\tilde{e}_{\mathrm{L}}^{\mp}$ and $\tilde{e}_{\mathrm{L}}^{+}\tilde{e}_{\mathrm{L}}^{-}$, followed by the decays $\tilde{e}_{\mathrm{L,R}}^{\pm} \to e^{\pm}\tilde{\chi}_1^0$ and $\tilde{e}_{\mathrm{L}}^{\mp} \to \nu_e\tilde{\chi}_1^{\mp} \to \nu_e\nu_\tau\tau^{\mp}\tilde{\chi}_1^0$. To a lesser extent, also pair production of charginos or neutralinos with subsequent (cascade) decays contributes.

In addition, pure standard model (SM) processes, in particular W-boson pair production (W^+W^-) and single

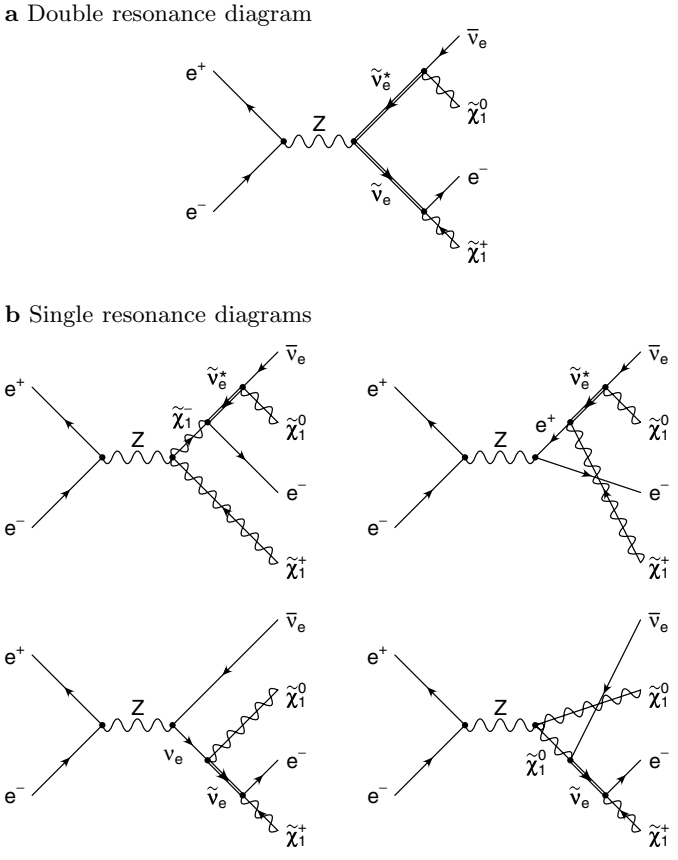

Fig. 3. The doubly and singly resonant contributions to the process $e^+e^- \to e^-\bar{\nu}_e\,\tilde{\chi}_1^0\,\tilde{\chi}_1^+$

W-boson production ($W^{\pm}e^{\mp}\nu_e$), leading to the final state $e^{\pm}\tau^{\mp}\nu_e\nu_\tau$, have to be taken into account. They are generically large and need to be reduced by appropriate cuts. Since the missing energy signature in the standard model background is generated by two neutrinos, which can be considered massless, but the sneutrino signal involves two additional massive neutralinos, a cut on the missing energy proves to be effective. In the SPS1a scenario, the sneutrino signal near threshold is concentrated at visible energies of $E_{\mathrm{vis}} \leq 0.15 \times \sqrt{s} \approx 60\,\mathrm{GeV}$, whereas the main background leads to much large values of the visible energy. Therefore the requirement $E_{\mathrm{vis}} \leq 0.15 \times \sqrt{s}$ reduces the background by about an order of magnitude, while leaving the sneutrino signal intact. In addition a few general cuts are applied to parametrize the acceptance regions of the detector and to reduce the background from soft events. The explicit values for the cuts are summarized in Table 2.

Additional acollinearity cuts [1,10], would not improve the signal-to-background ratio.

The signal rates can be further enhanced by using beam polarization. As evident from (2)–(4), the optimal polarization combination for $\tilde{\nu}_e$ production is a left-polarized e^- and a right-polarized e^+ beam; with realistic polarization degrees of 80% for electrons and 50% for positrons [11].

For this setup, we have calculated the threshold cross-section for electron-sneutrino production including the backgrounds from supersymmetric and standard model sources. The calculation is supplemented by initial-state

Table 2. Cuts to reduce the main standard model and SUSY backgrounds and to account for the detector geometry and resolution

Condition	Variable	Accepted range
Reject leptons in forward/backward region from Bhabha/Møller scattering	lepton polar angle θ_{l}	$\lvert\cos\theta_{\mathrm{l}}\rvert < 0.95$
Reject soft leptons/jets from radiative photon splitting and γ-γ background	lepton/jet energy E_{l}	$E_{\mathrm{l}} > 5\,\mathrm{GeV}$
Reject missing momentum in forward/backward region from particles lost in the beam pipe	missing momentum polar angle $\theta_{\boldsymbol{p}_{\mathrm{miss}}}$	$\lvert\cos\theta_{\boldsymbol{p}_{\mathrm{miss}}}\rvert < 0.90$
Angular separation between e and τ lepton	angle $\phi_{\mathrm{e}\tau}$ between electron and tau jet	$\lvert 1-\cos\phi_{\mathrm{e}\tau}\rvert > 0.015$
Reject events with large visible energy, mainly from SM background	visible energy $E_{\mathrm{vis}} = E_e + E_\tau$	$E_{\mathrm{vis}} \le 0.15 \times \sqrt{s}$

radiation (ISR) and beamstrahlung effects. The resulting excitation curve is depicted in Fig. 4, showing the final prediction for the signal with the backgrounds added on.

We estimate the precision for the sneutrino mass measurement from a threshold scan based on data simulated at 5 equidistant points in a center-of-mass energy range of 20 GeV in the threshold region for $\tilde{\nu}_e$ pair production, assuming a luminosity of $10\,\mathrm{fb}^{-1}$ per scan point. Since the backgrounds are sufficiently flat, they can be approximated by a straight line. Therefore the excitation curve can be fitted in a model-independent way by using four free parameters: the sneutrino mass and width, a constant scale factor for the absolute normalization of the excitation curve and a constant background level. The last two parameters render the fit independent on the details of the supersymmetric model, in particular the a priori unknown branching fractions of the sneutrinos. For the reconstruction of the mass a binned likelihood method is employed, where the likelihood variable is a function of the four parameters mentioned above. The fit result for the mass determination is finally

$$m_{\tilde{\nu}_e} = 186.0^{+1.1}_{-0.9}\,\mathrm{GeV}. \tag{16}$$

This demonstrates that the mass measurement at threshold is feasible with a precision of better than 1% and in fact surpasses the expected precision from decay energy spectra [4]. The result is not affected by the $\tilde{\nu}_e$ width in the theoretically expected range. For the decay width of the sneutrino only a wide upper bound can be set, $\Gamma_{\tilde{\nu}_e} \lesssim 0.9$ GeV.

4 Continuum production and Yukawa couplings

The precision analysis of sneutrino production in the continuum is used on the one hand to determine the sneutrino and chargino masses from the energy spectra of the decay products, a method complementary to the threshold scans [4].

In addition, it can be used to test the fundamental structure of the supersymmetric theory, the identity of the lepton-sneutrino–gaugino ($l\tilde{\nu}_l\tilde{W}$) Yukawa couplings with the associated lepton-neutrino–gauge boson ($l\nu_l W$) couplings of the first generation. The cross-section for $\tilde{\nu}_e$ pair production is sensitive to the Yukawa couplings through the t-channel chargino exchange. This section will address the theoretical techniques necessary for controlling the higher-order corrections and, subsequently, the phenomenological evaluation of the sneutrino cross-section measurement for the purpose of Yukawa coupling extraction.

4.1 Structure of one-loop corrections

For the general calculational techniques, the computer algebra tools and the regularization and renormalization of the MSSM at the one-loop level, the reader is referred to [1]. Here the framework will be extended to illuminate the specific points in the renormalization of sneutrinos. As before, the renormalization of masses and physical fields are performed in the on-shell scheme, i.e. the particle masses are identified with the physical propagator poles, and the on-shell physical fields are normalized to unity.

Since L-sneutrinos and charged L-sleptons are grouped together in an SU(2) doublet, the renormalization of neutral and charged sleptons must be treated conjointly. In the limit of vanishing lepton masses, the charged L- and R-sleptons do not mix, so that the R-slepton can be separated from the sneutrino and L-slepton states.

Since SU(2) invariance allows only for one soft supersymmetry breaking parameter $m_{\tilde{L}_{\mathrm{L}}}$ for the sneutrino and the charged L-slepton of one generation, the two masses are interdependent. Based on the tree-level relations between particle masses, soft-breaking terms and D-terms

$$m^2_{\tilde{l}_{\mathrm{L}}} = m^2_{\tilde{L}_{\mathrm{L}}} + M^2_{\mathrm{Z}}\cos 2\beta\,(-\tfrac{1}{2} + {s_{\mathrm{W}}}^2) + \mathcal{O}(m^2_{\mathrm{e}}), \tag{17}$$

$$m^2_{\tilde{\nu}_l} = m^2_{\tilde{L}_{\mathrm{L}}} + \tfrac{1}{2}M^2_{\mathrm{Z}}\cos 2\beta, \tag{18}$$

the L-sneutrino and L-slepton masses within each generation are related at Born level according to

$$m^2_{\tilde{\nu}_l} - m^2_{\tilde{l}_{\mathrm{L}}} = M^2_{\mathrm{W}}\cos 2\beta \quad [\text{Born level}]. \tag{19}$$

This relation is modified by higher-order corrections. Adopting the on-shell renormalization scheme for the slepton masses, the mass difference is shifted by a finite, but non-zero amount,

$$m^2_{\tilde{\nu}_l} - m^2_{\tilde{l}_{\mathrm{L}}} \to M^2_{\mathrm{W}}\cos 2\beta + \Delta m^2_{\tilde{\nu}_l}, \tag{20}$$

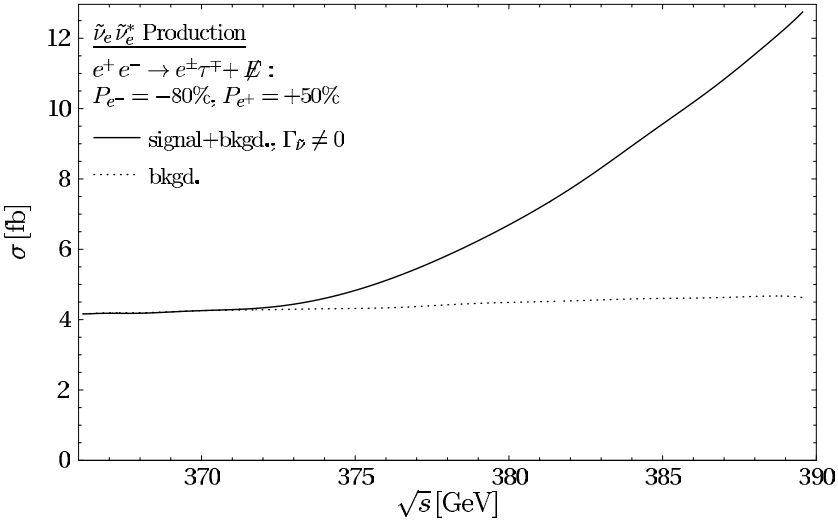

Fig. 4. The excitation curves for $\tilde{\nu}_e$ pair production over standard model and supersymmetric backgrounds for e^+e^- annihilation. The signal is enhanced with beam polarization as indicated, where (+) corresponds to right-handed and (−) to left-handed polarization

Table 3. Tree-level and one-loop corrected masses of the first and second generation sleptons for the SPS1a reference point [5]. The charged slepton masses are defined identical at tree and loop level in the on-shell scheme adopted here; the sneutrino mass is shifted correspondingly

	$\tilde{l}_R = \tilde{e}_R/\tilde{\mu}_R$	$\tilde{l}_L = \tilde{e}_L/\tilde{\mu}_L$	$\tilde{\nu}_l = \tilde{\nu}_e/\tilde{\nu}_\mu$
tree-level	142.72 GeV	202.32 GeV	185.99 GeV
one-loop			186.34 GeV

$$\Delta m^2_{\tilde{\nu}_l} = \Re e\Big\{\Sigma^{\tilde{l}_L}(m^2_{\tilde{l}_L}) - \Sigma^{\tilde{\nu}_l}(m^2_{\tilde{\nu}_l})\Big\} + \cos 2\beta\, \delta M_W^2 - M_W^2 \sin^2 2\beta\, \frac{\delta \tan\beta}{\tan\beta}. \quad (21)$$

$\hat{\Sigma}^{\tilde{l}_L,\tilde{\nu}_l}$ are the unrenormalized self-energies of the L-slepton and the sneutrino, respectively. Their UV-divergence is canceled by the counterterms for the W mass and the Higgs mixing term $\cos 2\beta$. Here the W mass is renormalized on-shell, while $\overline{\rm DR}$ renormalization is employed for the parameter $\tan\beta$ [1].

By fiat, the physical on-shell masses of the charged sleptons are identified with the Born-level masses. As a result, the sneutrino masses are shifted by the finite amount $\Delta m^2_{\tilde{\nu}_l} \equiv m^2_{\tilde{\nu}_l} - m^2_{\tilde{\nu}_l,\rm Born}$ from the corresponding Born value to the physical on-shell value through the one-loop corrections in (21). The sneutrino mass shift is exemplified in Table 3 for the reference point SPS1a.

In the calculation of the loop contributions it is necessary to use tree-level masses throughout in order to preserve gauge invariance[1]. For the phase-space integration, on the other hand, the matrix elements need to be expressed in terms of the physical masses for the external final-state sneutrinos. Both requirements can be technically realized by a systematic expansion of the complete loop corrected matrix element. Defining the matrix element $\mathcal{M}(m^2_{\tilde{\nu}}, m^2_{\tilde{\nu}})$ as a function of the physical masses of the two produced sneutrinos and expanding it around the Born sneutrino masses yields

$$\mathcal{M}(m^2_{\tilde{\nu}}, m^2_{\tilde{\nu}}) = \mathcal{M}(m^2_{\tilde{\nu},\rm Born}, m^2_{\tilde{\nu},\rm Born}) + \Delta m^2_{\tilde{\nu}} \left[\frac{\partial}{\partial m^2_{\tilde{\nu}}} \mathcal{M}(m^2_{\tilde{\nu}}, m^2_{\tilde{\nu}})\right]_{m^2_{\tilde{\nu}} = m^2_{\tilde{\nu},\rm Born}} + \mathcal{O}(\Delta m^4_{\tilde{\nu}}). \quad (22)$$

Expanding this expression up to next-to-leading order in perturbation theory and observing that $\Delta m^2_{\tilde{\nu}}$ represents already a one-loop contribution then leads to

$$\mathcal{M}(m^2_{\tilde{\nu}}, m^2_{\tilde{\nu}}) = \mathcal{M}_{(0)}(m^2_{\tilde{\nu},\rm Born}, m^2_{\tilde{\nu},\rm Born}) + \mathcal{M}_{(1)}(m^2_{\tilde{\nu},\rm Born}, m^2_{\tilde{\nu},\rm Born}) + \Delta m^2_{\tilde{\nu}} \left[\frac{\partial}{\partial m^2_{\tilde{\nu}}} \mathcal{M}_{(0)}(m^2_{\tilde{\nu}}, m^2_{\tilde{\nu}})\right]_{m^2_{\tilde{\nu}} = m^2_{\tilde{\nu},\rm Born}} + \text{higher orders}, \quad (23)$$

where the indices in parentheses indicate the loop order. As evident from (23), the next-to-leading corrections receive two contributions: the one-loop corrections to the sneutrino production matrix element, $\mathcal{M}_{(1)}$, with Born masses in all loop expressions, and a contribution originating from the one-loop mass shift of the sneutrinos.

Note that the shift $\Delta m^2_{\tilde{\nu}}$, beyond its role in the present theoretical context, can in principle be experimentally accessed directly through precision measurements of the sneutrino and selectron masses. With the expected precision of $m_{\tilde{\nu}_e}$ and given the per-mill accuracy of $m_{\tilde{e}_L}$, the measured difference of the physical masses $m_{\tilde{\nu}_e} - m_{\tilde{e}_L}$ starts to become sensitive to the quantum correction $\Delta m^2_{\tilde{\nu}}$.

A finite mass shift similar to (21) arises for all scalar partners of the left-handed standard model fermions, i.e. also for the squark sector. It may be noted that while these sfermion mass shifts do affect the one-loop calculation of sfermion production, they need not be taken into account for the one-loop corrections to sfermion decays presented in [12], since the Born matrix elements for sfermion decays do not depend on the mass of the decaying sfermion.

In many facets, the radiative corrections to sneutrino production are characteristic for sparticle production processes. In particular, supersymmetric loop contributions

[1] This feature has been checked explicitly by using a general covariant R_ξ gauge and verifying the gauge-parameter independence of the total result.

can lead to corrections that do not decouple for large superpartner masses [13,14]. While in general quantum effects are reduced with increasing mass of the virtual particles, broken symmetries giving rise to mass splittings within particle multiplets elude this argument. Accordingly, the breaking of supersymmetry can generate corrections that grow logarithmically with the mass splitting between SM particles and their SUSY partners.

In slepton production, non-decoupling SUSY effects can arise in the loop corrections to lepton-slepton-gaugino Yukawa vertices, leading to logarithmically enhanced effective Yukawa couplings [1, 15], while the gauge boson vertices are protected by gauge invariance. Therefore only the production matrix elements of first-generation sneutrinos, i.e. $\tilde{\nu}_e\tilde{\nu}_e^*$ production, involving t-channel chargino exchange, are affected by non-decoupling corrections from other SUSY particles. Potentially large corrections can arise in particular from virtual quark and squark loops for very large squark masses, so that sneutrino cross-sections can be sensitive to high squark mass scales [16].

In addition to the matrix elements of the production cross-sections, non-decoupling SUSY corrections typically also occur in the loop corrections to the mass matrices of the superpartners. These corrections are reflected in shifts to mass relations, such as the sneutrino mass shift $\Delta m_{\tilde{\nu}}$ in (21).

Another remarkable property is the appearance of anomalous threshold singularities within vertex and box diagrams [1], which show up as discontinuities in the cross-section as a function of the center-of-mass energy. Anomalous thresholds correspond to configurations in a vertex loop correction, for instance, where all particle lines become on-shell simultaneously, which is easily kinematically realizable in SUSY theories as a consequence of the diversified sparticle spectrum [1].

4.2 Production cross-sections

The complete virtual $\mathcal{O}(\alpha)$ corrections, as outlined above, are renormalized using the on-shell definition for all masses, while the electromagnetic coupling α is evaluated at the scale of the center-of-mass energy $Q = \sqrt{s}$, so that the large logarithmic corrections $\propto \log s/m_f^2$ from light fermion loops in the running of $\alpha(Q^2)$ are absorbed automatically.

The resulting UV-finite amplitude still contains infrared divergences from virtual photon exchange, which are absorbed by adding the contributions from real photon radiation to the cross-section. Since the final-state sneutrinos are neutral, photon radiation can only occur in the initial state and from internal charged particle lines; see Fig. 5.

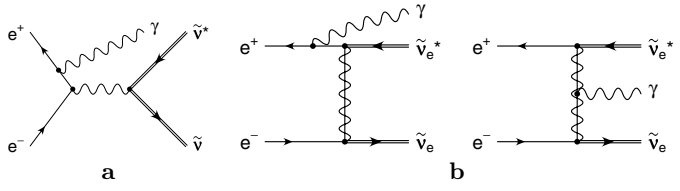

Fig. 5. Feynman diagrams for real photon emission in sneutrino production, with **a** contributing to all sneutrino flavors, while **b** only applies for electron-sneutrino production

In the case of $\tilde{\nu}_\mu$ and $\tilde{\nu}_\tau$ pair production, the analysis is simple since the virtual and real (initial-state) QED corrections form a gauge-invariant subset independent from the other virtual corrections. The QED contributions arising from virtual and soft real photon radiation are proportional to the Born cross-section,

$$\begin{aligned} &\mathrm{d}\sigma_{\mathrm{virt+soft}}[e^+e^- \to \tilde{\nu}_l\,\tilde{\nu}_l^*] \\ &= \mathrm{d}\sigma_{\mathrm{Born}}[e^+e^- \to \tilde{\nu}_l\,\tilde{\nu}_l^*] \times \delta^l_{\mathrm{virt+soft}}, \end{aligned} \tag{24}$$

$$\begin{aligned} &\delta^l_{\mathrm{virt+soft}} \\ &= \frac{\alpha}{\pi}\left[\log\frac{4(\Delta E)^2}{s}\left(\log\frac{s}{m_{\mathrm{e}}^2}-1\right)\right. \\ &\quad \left. +\frac{3}{2}\,\log\frac{s}{m_{\mathrm{e}}^2}-2+\frac{\pi^2}{3}\right] \qquad [l \neq e]. \end{aligned} \tag{25}$$

The dependence on the cut-off ΔE for the soft-photon energy is removed when the radiation of hard photons is added to the cross-section.

The loop calculation to $\tilde{\nu}_e$ pair production is considerably more complex due to the additional t-channel chargino exchange mechanism. Besides a large set of additional diagrams, the diagrams involving gauge bosons, Higgs bosons, gauginos and higgsinos cannot be separated from the QED loops in a gauge-invariant and UV-finite way anymore. The photonic corrections to the electron-sneutrino-chargino Yukawa vertex becomes UV-finite only after being supplemented by the corresponding photino loop diagram. Since the photino is not a mass eigenstate, this amplitude is intrinsically linked to the remaining degrees of freedom in the gauge sector. Thus only the total set of gauge boson/Higgs and gaugino/higgsino electroweak diagrams is gauge invariant.

Nevertheless, the size of the genuinely process-specific corrections can be characterized by the following definition. Subtracting, from the virtual and soft corrections, the leading logarithmic terms $\propto \log(\Delta E)^2/s$ and $\propto \log s/m_{\mathrm{e}}^2$, which are generated by infrared/collinear photon emission plus virtual photon corrections, the remaining corrections are gauge invariant and free of logarithmically enhanced terms.

The overall next-to-leading order corrections to the total cross-section for sneutrino-pair production are presented in Fig. 6. The parameters of the Snowmass reference point SPS1a have been adopted again to illustrate the final results. The corrections are normalized to the Born cross-section, defined with the running electromagnetic coupling.

In addition to the full corrections, the result for $\tilde{\nu}_\mu$ pair production is divided into QED corrections and the remaining contributions from massive virtual loops. Also shown separately is the effect of the one-loop shift to the sneutrino mass in (21) in addition to the radiative corrections to the matrix element $\mathcal{M}_{(1)}$ in (23). The sneutrino mass shift does not only modify the next-to-leading order matrix element according to (23), but is also crucial for defining the proper sneutrino mass in the physical phase-space kinematics.

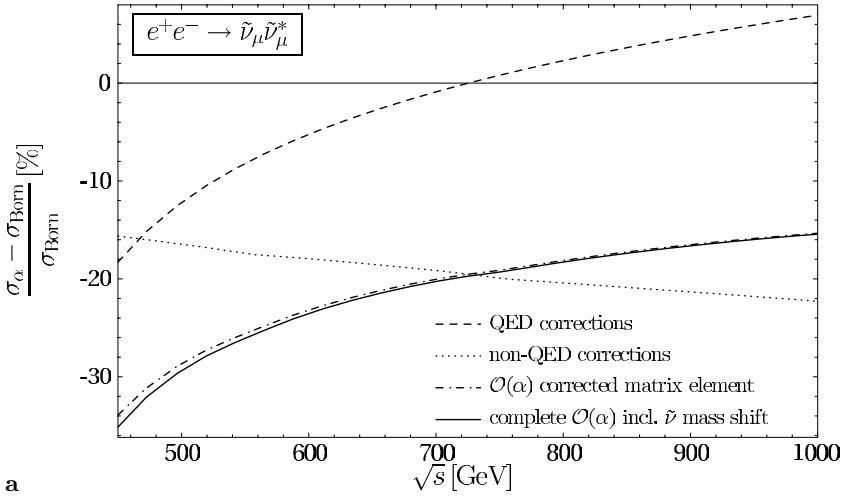

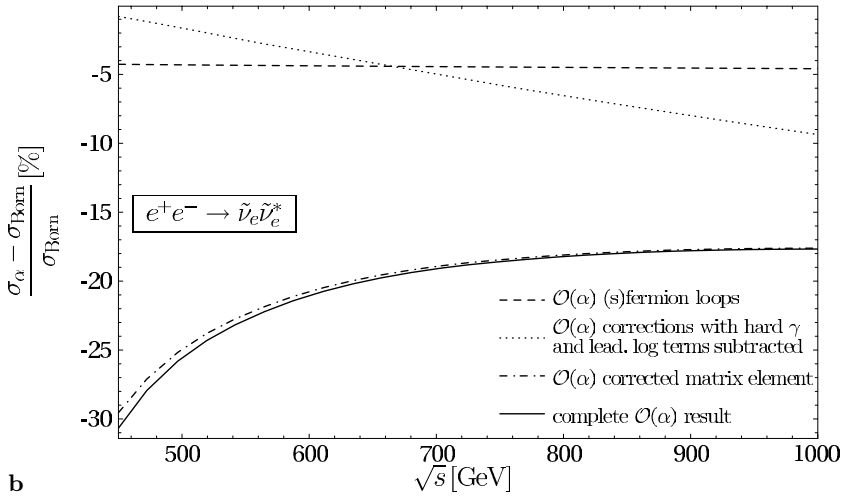

Fig. 6. Electroweak corrections to the cross-sections **a** for $e^+e^- \to \tilde{\nu}_\mu \tilde{\nu}_\mu^*$ and **b** for $e^+e^- \to \tilde{\nu}_e \tilde{\nu}_e^*$, relative to the improved Born cross-section. Besides the full $\mathcal{O}(\alpha)$ result, contributions from different subsets of diagrams are shown, in particular the genuinely process-specific corrections defined by subtracting hard photon radiation and leading-log soft and virtual photon effects from the overall $\mathcal{O}(\alpha)$ corrections. Input parameters taken from the SPS1a scenario

For $\tilde{\nu}_e$ pair production the complete QED subset of the $\mathcal{O}(\alpha)$ corrections cannot be extracted in a gauge-invariant and UV-finite manner. Nevertheless, one can identify a gauge-invariant individual contribution from closed loops of fermions and/or sfermions, as shown in Fig. 6b. In addition, the dominant QED corrections can be characterized by the hard photon radiation and the leading logarithmic soft and virtual contributions. The remaining non-QED logarithmically regularized corrections are also depicted in Fig. 6b.

Both for $\tilde{\nu}_\mu$ and $\tilde{\nu}_e$ pair production, the contribution of the sneutrino mass shift is relatively small. The total next-to-leading order corrections, however, are large, between 20 and 30%. As can be inferred from Fig. 6a, these large effects do not only originate from the QED corrections, which contain large collinear logarithms $\propto \log s/m_{\rm e}^2$; see (25). In fact, the massive non-photonic virtual loops also generate corrections of about 10% or more.

In the following, the influence of the corrections induced through the supersymmetry sector itself shall be studied in some detail. In Figs. 7a,b, the effect of the parameters in the electroweak gaugino sector on the one-loop corrections is exemplified in regard to the parameters M_2 and μ. The effects are significant both for $\tilde{\nu}_\mu$ and $\tilde{\nu}_e$ pair production, with variations in the cross-section of several per-cent, up to about 10%. The abrupt changes along the diagonal $M_2 = \mu$ for $\tilde{\nu}_e$ pair production in Fig. 7b are a consequence of the level crossings between the $\tilde{\chi}_i^\pm$ states.

As outlined above, large mass splittings between the SUSY sfermions and the corresponding SM fermions generate large non-decoupling corrections to the effective Yukawa couplings and thus to $\tilde{\nu}_e \tilde{\nu}_e^*$ production. This can be illustrated by comparing the squark loop effect on the $\tilde{\nu}_\mu$ pair cross-sections, where supersymmetric Yukawa interactions are absent at the Born level, with the $\tilde{\nu}_e$ pair cross-section mediated by t-channel chargino exchange.

Beyond the low-energy region, which is affected by various thresholds, the radiative loop contributions are expected to rise proportional to the logarithm $\log M_{\tilde{\rm Q}}$ of the squark masses for $\tilde{\nu}_e$ production, while approaching a plateau for $\tilde{\nu}_\mu$ production. This is borne out in the evolution of the full lines in Fig. 8a,b.These curves are generated for fixed physical masses of $\tilde{\nu}_\mu$ and $\tilde{\nu}_e$. However, as demonstrated by the dashed line in Fig. 8a, a small logarithmic effect is induced also in $\tilde{\nu}_\mu$ pair production if the soft-breaking parameter $m_{\tilde{L}_{\rm L}}$ is kept fixed. In this scheme the physical $\tilde{\nu}_\mu$ mass is shifted by the one-loop corrections in (21), effecting non-decoupling contributions logarithmic in $M_{\tilde{\rm Q}}$.

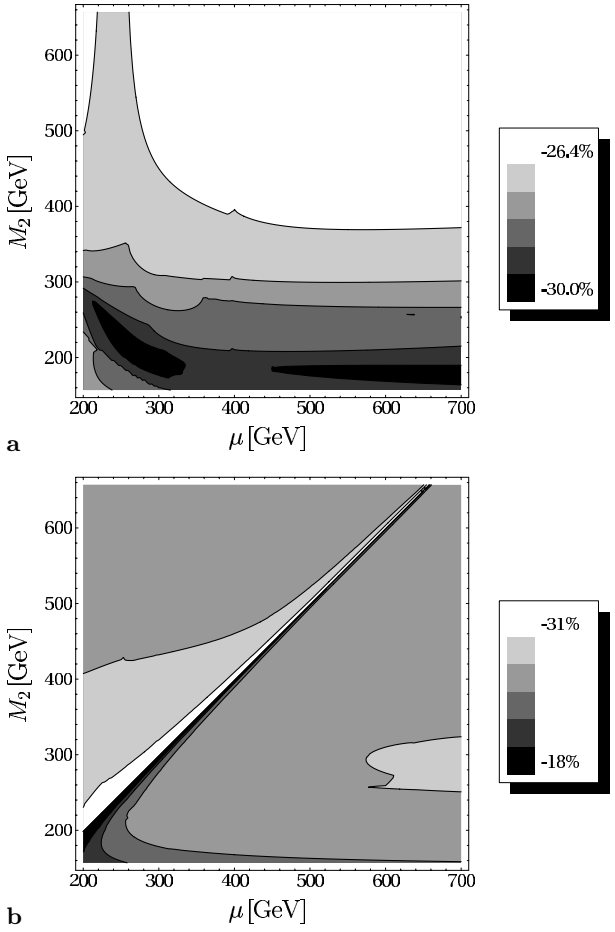

Fig. 7. Dependence of the relative one-loop corrections $(\sigma_\alpha - \sigma_{\rm Born})/\sigma_{\rm Born}$ to $\tilde{\nu}_\mu\tilde{\nu}_\mu^*$ production **a** and $\tilde{\nu}_e\tilde{\nu}_e^*$ production **b** on the gaugino parameters M_2 and μ for $\sqrt{s} = 500\,\text{GeV}$. The values of the other parameters are taken from the SPS1a scenario

On the other hand, the squark loop contributions to $\tilde{\nu}_e\tilde{\nu}_e^*$ production generate relatively large effects in the effective supersymmetric Yukawa vertices, with variations of several per-cent for squark masses of $\mathcal{O}(1\,\text{TeV})$; cf. Fig. 8b. This significantly different behavior could be used to constrain the parameters of a very heavy squark sector, that escapes direct detection, through the precise measurement of the $\tilde{\nu}_e\tilde{\nu}_e^*$ cross-section, as advocated in [16].

4.3 The identity of Yukawa and gauge couplings

The analysis of electron-sneutrino production provides an important testing ground for the identity of electroweak SUSY Yukawa couplings and the corresponding SM gauge couplings. This identity can also be tested in neutralino [17] and selectron [1] pair production, which involve electron–selectron–neutralino ($e\tilde{e}\tilde{\chi}^0$) Yukawa interactions. While these channels are sensitive to a mixture of SU(2) and U(1) SUSY Yukawa couplings, corresponding to the wino and bino components of the neutralinos, there is no U(1) component contributing to sneutrino-pair production, thus allowing for direct access to the SU(2) ($e\tilde{\nu}_e\tilde{W}$) Yukawa coupling. Moreover, the chargino mixing structure is substantially simpler than the neutralino mixing, thus simplifying the analysis for $\tilde{\nu}_e$ pair production compared to $\tilde{e}$ pair production. This is analogous to probing the SU(2) Yukawa coupling in chargino pair production, which provides a complementary experimental method [17].

In our analysis, we will assume that the masses and mixing parameters of the charginos can be determined independently from chargino pair production, and appropriate estimates of the errors for these quantities are included. Essentially, only the gaugino/higgsino mass parameters M_2 and μ of the chargino system are important in the sneutrino analysis. The influence of $\tan\beta$ on the sneutrino cross-section is rather weak, so that knowledge of $\tan\beta$ to within a factor of two is sufficient. In this case, the MSSM parameters M_2 and μ can be determined from precision measurements of the lighter chargino $\chi_1^\pm$ and neutralino $\tilde{\chi}_{1,2}^0$ masses.

As elaborated in the previous section, the one-loop corrections to the production cross-section are sizeable and they need to be taken into account for any precision measurement. In principle this will introduce a dependence of the cross-section prediction on *all* MSSM parameters entering in the loops, including their measurement errors. However, the results can be calculated for ideal values of the parameters of the squark, charged slepton, Higgs and neutralino sectors, since their errors would affect the errors in the Yukawa couplings only to second order. For the parameters present already in the Born approximation, i.e. the sneutrino and chargino parameters, errors are taken into account properly. Iterative procedures may later be employed for the next-level improvements.

Besides the chargino parameters, the cross-section depends strongly on the sneutrino masses, which can be extracted from a threshold scan; see (16). The chargino parameters are extracted from mass measurements of the light chargino and neutralino states, assuming the following errors, $\delta m_{\tilde{\chi}_1^0} = 50\,\text{MeV}$, $\delta m_{\tilde{\chi}_2^0} = 80\,\text{MeV}$, $\delta m_{\tilde{\chi}_2^\pm} = 3000\,\text{MeV}$, which are based on a coherent analysis of LHC and LC mass measurements [18].

The $\tilde{\nu}_e\tilde{\nu}_e^*$ production cross-section is computed using the beam polarizations and cuts introduced in Sect. 3, and including beamstrahlung and ISR effects. Besides increasing the statistics, the polarization of both the e^- and e^+ beams is a tool for testing the chiral quantum numbers of the sneutrinos. In fact, in the SUSY Yukawa interactions, $\tilde{\nu}_e$ only couples to left-handed electrons, while $\tilde{\nu}_e^*$ only couples to right-handed positrons. It is assumed that the polarization degree of the incoming electron/positron beams can be determined with an error of 1% [11]. Detector effects are approximated by assigning a simple global acceptance factor of $\epsilon_{\rm det} = 50\%$. The numerical analysis in the SPS1a scenario is based on 500 fb^{-1} data accumulated in e^+e^- collisions at $\sqrt{s} = 500\,\text{GeV}$.

Taking into account all the constraints and error sources mentioned above, the following 1σ error for the extraction of the SU(2) Yukawa coupling from the cross-section measurement is obtained:

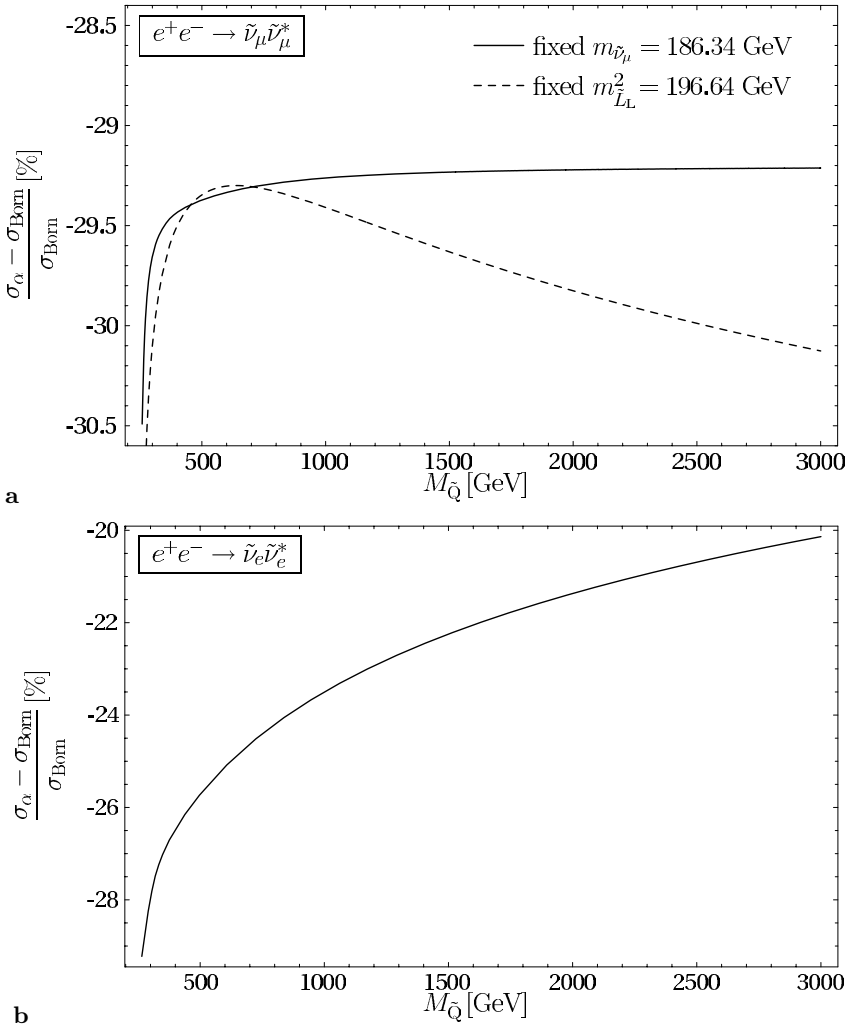

Fig. 8. Dependence of the one-loop corrections on the soft-breaking squark mass parameter $M_{\tilde{Q}}$ [assumed to be universal for all squarks] for $\tilde{\nu}_\mu \tilde{\nu}^*_\mu$ production **a** and $\tilde{\nu}_e \tilde{\nu}^*_e$ production **b**. In panel **a** the dashed line corresponds to a fixed L-smuon soft-breaking parameter $m^2_{\tilde{L}_L} = 196.64\,\text{GeV}$ [6] as input, while for the full line the physical sneutrino mass $m_{\tilde{\nu}_\mu} = 186.34\,\text{GeV}$ is kept fixed. The values of the other parameters are taken from the SPS1a scenario, and the cms energy is set to $\sqrt{s} = 500\,\text{GeV}$

$$\delta\hat{g}/\hat{g} \approx 5\%, \tag{26}$$

where $\hat{g}$ is the SU(2) $e^\pm \tilde{\nu}_e^{(*)} \tilde{\chi}_i^\mp$ Yukawa coupling.

The precision does not reach the expected sensitivities for the extraction of the electroweak Yukawa couplings from selectron production [1, 15, 19], but the sneutrino channel has a less model-dependent base. The main source of uncertainty contributing to the error (26) is the sneutrino mass measurement, see (16), which due to the dominant invisible decay channel of the sneutrinos is less precise than for selectrons. The relatively large error is therefore a specific feature of the SPS1a scenario and the particular sneutrino decay spectrum. In other scenarios, the determination of the SUSY Yukawa coupling $\hat{g}$ from the sneutrino cross-section can improve considerably; see e.g. [16].

In summary, it turns out that the analysis of electron-sneutrino pair production at e^+e^- colliders can test the fundamental identity of Yukawa and gauge couplings in supersymmetric theories at the level of a few per-cent.

5 Conclusions

This report extends previous work in [1] on precision studies of scalar leptons at future linear colliders, by analyzing the sector of neutral scalar leptons. We have studied the pair production of sneutrinos in e^+e^- collisions, discussing the theoretical basis and drawing the phenomenological consequences for the determination of the masses and couplings of these particles.

The clean environment of high-energy lepton colliders operating with polarized beams at high luminosity allows one to measure the properties of SUSY particles with high precision. From a scan of the production cross-section near threshold, the *mass of the electron-sneutrino* $m_{\tilde{\nu}_e}$ can be determined with unparalleled precision due to the characteristic rise of the excitation curve with the third power in the sparticle velocity.

In order to provide a reliable theoretical description of the threshold cross-section, it is necessary to include non-zero width effects in a consistent way. The analysis is complicated by the fact that in typical mSUGRA-inspired MSSM scenarios, the sneutrino dominantly decays invisibly. Nevertheless, it could be shown that a significant signal can be extracted by combining one visible with one invisible decay mode of the sneutrino pair, and that backgrounds both from standard model and supersymmetric sources can be sufficiently reduced.

Using these elements, a phenomenological analysis of slepton masses in threshold scans was performed. Despite the impact of the relative low signal rate and remaining subdominant backgrounds, a precision of better than the per-cent level for the electron-sneutrino mass determination can be reached. The threshold fit can also be used to experimentally constrain the total decay width of the electron-sneutrino, but the accuracy would not suffice to establish significant experimental evidence for a non-zero sneutrino width.

The measurement of the electron-sneutrino cross-section can also be exploited to test the fundamental equality of the *Yukawa couplings* $\hat{g}(e\tilde{\nu}_e\tilde{W})$ of the electron, the sneutrino and the SU(2) gauginos, and the corresponding gauge couplings $g(e\nu_e W)$ of the electrons and electron-neutrinos to the W gauge bosons. Due to the chargino t-channel exchange, electron-sneutrino pair production is sensitive to the SUSY SU(2) Yukawa coupling. Based on a careful analysis of statistical errors and systematic uncertainties, we found that the SU(2) Yukawa coupling can be extracted at the few per-cent level or better from total cross-section measurements in the high-energy continuum.

Accordingly, the theoretical predictions for the cross-sections need to be calculated to the per-cent level to match this expected experimental accuracy. To this end, the complete next-to-leading order SUSY electroweak corrections have been calculated for the production of on-shell sneutrino pairs in the continuum. These one-loop corrections can be relatively large, up to the order of 20–30%, with genuine SUSY loop contributions leading to sizeable effects of a few per-cent. Thus the sneutrino-pair production cross-sections are significantly affected by parameters of other SUSY sectors, which must be introduced in systematic iterative procedures.

We have implemented the results into computer programs, that are available on the web at http://theory.fnal.gov/people/afreitas/. [Technical information on installing and running the programs are given at this web site.]

A self-consistent analysis of the SUSY sector at the expected experimental precision will eventually have to take into account the impact of the parameters of all SUSY sectors in the theoretical predictions at the loop level. Accordingly, a coherent study of many different channels in parallel – sleptons, charginos/neutralinos and squarks/gluinos – has to be performed [20]. Such a comprehensive study is currently pursued in the context of the SPA Project [21], and will ultimately establish the access to the fundamental supersymmetric theory and its microscopic breaking mechanism at potentially high scales.

Acknowledgements. We benefited from very helpful communication with H.U. Martyn and U. Nauenberg on experimental sneutrino analyses at e^+e^- linear colliders. We are also very grateful to G.A. Blair for the careful reading of the manuscript.

References

1. A. Freitas, A. von Manteuffel, P.M. Zerwas, Eur. Phys. J. C **34**, 487 (2004)
2. A. Arhrib, W. Hollik, JHEP **0404**, 073 (2004); K. Kovařík, C. Weber, H. Eberl, W. Majerotto, Phys. Lett. B **591**, 242 (2004)
3. G.A. Blair, W. Porod, P.M. Zerwas, Eur. Phys. J. C **27**, 263 (2003) [hep-ph/0210058]
4. U. Nauenberg, contribution to the 3rd Workshop of the Extended ECFA/DESY Linear Collider Study, Prague, Czech Republic (2002)
5. B.C. Allanach et al., Eur. Phys. J. C **25**, 113 (2002)
6. N. Ghodbane, H.U. Martyn, in Proceedings of the APS/DPF/DPB Summer Study on the Future of Particle Physics (Snowmass 2001), edited by R. Davidson, C. Quigg [hep-ph/0201233]
7. A. Freitas, D.J. Miller, P.M. Zerwas, Eur. Phys. J. C **21**, 361 (2001)
8. A. Freitas, A. v. Manteuffel, in Proceedings of the 10th International Conference on Supersymmetry and Unification of Fundamental Interactions (SUSY02), edited by P. Nath, P.M. Zerwas, Hamburg, Germany (2002) [hep-ph/0211105]
9. J.K. Mizukoshi, H. Baer, A.S. Belyaev, X. Tata, Phys. Rev. D **64**, 115017 (2001)
10. H.-U. Martyn, in Conceptual Design of a 500 GeV e^+e^- Linear Collider, edited by R. Brinkmann, G. Materlik, J. Rossbach, A. Wagner, DESY 1997-048, ECFA 1997-182
11. G. Moortgat-Pick, H.M. Steiner, Eur. Phys. J. direct C **3**, 6 (2001)
12. J. Guasch, W. Hollik, J. Solà, Phys. Lett. B **510**, 211 (2001); JHEP **0210**, 040 (2002)
13. M.M. Nojiri, K. Fujii, T. Tsukamoto, Phys. Rev. D **54**, 6756 (1996)
14. H.C. Cheng, J.L. Feng, N. Polonsky, Phys. Rev. D **56**, 6875 (1997); M.M. Nojiri, D.M. Pierce, Y. Yamada, Phys. Rev. D **57**, 1539 (1998); E. Katz, L. Randall, S. Su, Nucl. Phys. B **536**, 3 (1998)
15. H.C. Cheng, J.L. Feng, N. Polonsky, Phys. Rev. D **57**, 152 (1998)
16. M.M. Nojiri, D.M. Pierce, Y. Yamada, Phys. Rev. D **57**, 1539 (1998)
17. S.Y. Choi, A. Djouadi, M. Guchait, J. Kalinowski, H.S. Song, P.M. Zerwas, Eur. Phys. J. C **14**, 535 (2000); S.Y. Choi, J. Kalinowski, G. Moortgat-Pick, P.M. Zerwas, Eur. Phys. J. C **22**, 563 (2001)
18. LHC/LC Study Group Working Report, edited by G. Weiglein et al., in preparation; K. Desch, J. Kalinowski, G. Moortgat-Pick, M.M. Nojiri, G. Polesello, JHEP **0402**, 035 (2004)
19. J.L. Feng, M.E. Peskin, H. Murayama, X. Tata, Phys. Rev. D **52**, 1418 (1995)
20. R. Lafaye, T. Plehn, D. Zerwas, SFITTER: SUSY parameter analysis at LHC and LC, hep-ph/0404282; P. Bechtle, K. Desch, P. Wienemann, Sfittino program code, to be published
21. Supersymmetry Parameter Analysis (SPA) Project, http://spa.desy.de/spa/